Available online at www.sciencedirect.com

ScienceDirect

Ceramics International 40 (2014) 375–384

CERAMICS INTERNATIONAL

www.elsevier.com/locate/ceramint

Magnetic nanocomposite based on titania–silica/cobalt ferrite for photocatalytic degradation of methylene blue dye

F.A. Harraz[a,c,*], R.M. Mohamed[a,b], M.M. Rashad[a], Y.C. Wang[d], W. Sigmund[d]

[a]*Advanced Materials Technology Department, Central Metallurgical Research and Development Institute, P.O. Box: 87, Helwan, Cairo 11421, Egypt*

[b]*Chemistry Department, Faculty of Science, King Abdulaziz University, P.O. Box 80203, Jeddah 21589, Saudi Arabia*

[c]*Promising Centre for Sensors and Electronic Devices (PCSED), Advanced Materials and Nano-Research Centre, Najran University, P.O. Box 1988, Najran 11001, Saudi Arabia*

[d]*Materials Science and Engineering Department, University of Florida, UF, Gainesville 32611, Fl, USA*

Received 26 May 2013; received in revised form 3 June 2013; accepted 3 June 2013
Available online 15 June 2013

Abstract

Magnetic photocatalysts were successfully prepared by coating titania–silica (TiO_2–SiO_2) on cobalt ferrite ($CoFe_2O_4$) nanoparticles. A simple organic acid precursor method was employed to prepare the magnetic part, while the TiO_2–SiO_2 was synthesized and coated onto $CoFe_2O_4$ by the sol–gel technique. Controlling the modification process of TiO_2–SiO_2 with $CoFe_2O_4$ nanoparticles is a key factor for obtaining appropriate catalytic performance. Under optimized conditions, a core–shell structure could be obtained in which $CoFe_2O_4$ is a core while TiO_2–SiO_2 forms a shell. The current photocatalyst exhibits remarkable catalytic activity for the degradation of methylene blue dye in water under UV irradiation. It was demonstrated that the catalyst could remove as high as 98.3% of the organic dye in just 40 min. The degradation efficiency was found to depend essentially on initial dye concentration, solution pH and the catalyst loading. The as-synthesized catalyst was characterized by different techniques including X-ray diffraction (XRD), X-ray photoelectron spectroscopy (XPS), Scanning electron microscopy (SEM), transmission electron microscopy (TEM), Fourier transform infrared (FT-IR) spectroscopy and N_2 adsorption–desorption isotherm. The photocatalyst could be removed from the reaction mixture and its recyclability remains effective and active after six cycles.

Keywords: A. Sol–gel processes; B. Nanocomposites; C. Magnetic properties; D. TiO_2

1. Introduction

Surface coating of nanoparticles with various materials to form core–shell morphologies is often used for development of catalysts and the optoelectronic devices [1–3]. Core–shell structures have been used as precursors to prepare hollow structures by the complete removal of core materials through chemical etching or combustion, and partial elimination of the core have enabled preparation of novel nanostructures inside the shell [4–6]. However, semiconductor photocatalysts have recently attracted much interest due to the potential applications of detoxification of environmental pollutants [7,8]. Particularly, the importance of degradation of organic contaminations using semiconductors photocatalysts has stimulated wide efforts to develop methods for their synthesis and characterization, making this area of study an integral part of photocatalysis [9–12].

Among the photocatalysts, titania (TiO_2) is the widely used semiconductor material because of its superior photoreactivity, nontoxicity, long-term stability, and low price. The photocatalytic activity of TiO_2 depends on various parameters, including crystallinity, impurities, surface area, and density of surface hydroxyl groups. Generally, TiO_2 could be used as a photocatalyst in both anatase and rutile crystal structures. Anatase phase has a much higher activity than rutile [13]. Nanocrystalline anatase has been used for degradation of

*Corresponding author at: Advanced Materials Technology Department, Central Metallurgical Research and Development Institute, P.O. Box 87, Helwan, Cairo 11421, Egypt. Tel.: +20 225010642; fax: +20 225010639.
E-mail addresses: fharraz68@yahoo.com, fharraz@cmrdi.sci.eg (F.A. Harraz).

0272-8842/$ - see front matter © 2013 Elsevier Ltd and Techna Group S.r.l. All rights reserved.
http://dx.doi.org/10.1016/j.ceramint.2013.06.012

undesirable organics in air or liquid phase [14,15]. Further, TiO_2 slurry is the frequently applied method to deal with pollutants in water due to its high specific surface area and good dispersion [16]. However, the use of TiO_2 slurry is still limited due to the difficulty to separate TiO_2 particles from the treated water [17]. One way to enhance the separation of catalyst is mixing TiO_2 with silica (SiO_2) as a support to increase the surface area, improve the photocatalytic activity and facilitate the separation and recovery of the catalyst [18]. Another strategy to overcome the separation limitation of catalyst is to modify the TiO_2 surface by depositing them onto magnetic nanoparticles [19–22].

Among the magnetic particles, spinel ferrite structures (AFe_2O_4) (where A is a divalent cation: Mn, Cu, Co, Mg, Co, Ni, Fe …etc.) have been coated with TiO_2 to synthesize magnetic nanocomposites to enhance the recovery of the catalyst and re-use it for several times from the treated water by applying an external magnetic field [23–25]. The popular magnetic material is the ferrite, because of its strong ferromagnetism and ease of preparation [26–28]. Chung et al. [29] synthesized a magnetic photocatalyst of nickel ferrite ($NiFe_2O_4$) coated with TiO_2 or TiO_2–SiO_2, by a multi-step ultrasonic spray pyrolysis with an aim to obtain a core–shell structure. However, a non-uniform coating on the surface of the magnetic cores was obtained; instead they formed patches on the surface, which resulted in decreasing the recycling of the magnetic photocatalyst. Zhang et al. [30] prepared a magnetic photocatalyst of titania coating on silica and modified with cobalt ferrite. They prepared the photocatalyst via hydrolysis and condensation of water-soluble titanium bis-ammonium lactato dihydroxide at low temperature and employed the catalyst for the degradation of methyl orange. However, neither the factors affecting the photodegradation process nor the recyclability of the photocatalyst was investigated.

The aim of the present work is to provide a solid base of knowledge for the synthesis of well defined nanocomposites based on TiO_2–SiO_2/$CoFe_2O_4$ that have remarkable photocatalytic activity together with superior magnetic properties. The as-synthesized magnetic photocatalyst is applied for the degradation of methylene blue (MB) dye in aqueous solutions as a model pollutant. Results of catalyst synthesis and characterization and its catalytic performance evaluation are thoroughly addressed and discussed in this paper.

2. Experimental

2.1. Catalyst synthesis

The applied procedure for the synthesis of TiO_2–SiO_2/$CoFe_2O_4$ magnetic photocatalyst is schematically depicted in the flowchart of Fig. 1. Cobalt ferrite nanoparticles were firstly prepared using aqueous solutions of $FeCl_3 \cdot 6H_2O$ and $Co(NO_3)_2 \cdot 6H_2O$ with a molar ratio Fe^{3+}:Co^{2+} = 2:1 in presence of oxalic acid according to our earlier work [31]. The solution was stirred and evaporated at 80 °C until a clear, viscous gel was obtained, and then dried at 110 °C for 24 h. The powder was then calcined in air at 1000 °C for 2 h. Synthesis of $CoFe_2O_4$/TiO_2–SiO_2 nanocomposites were

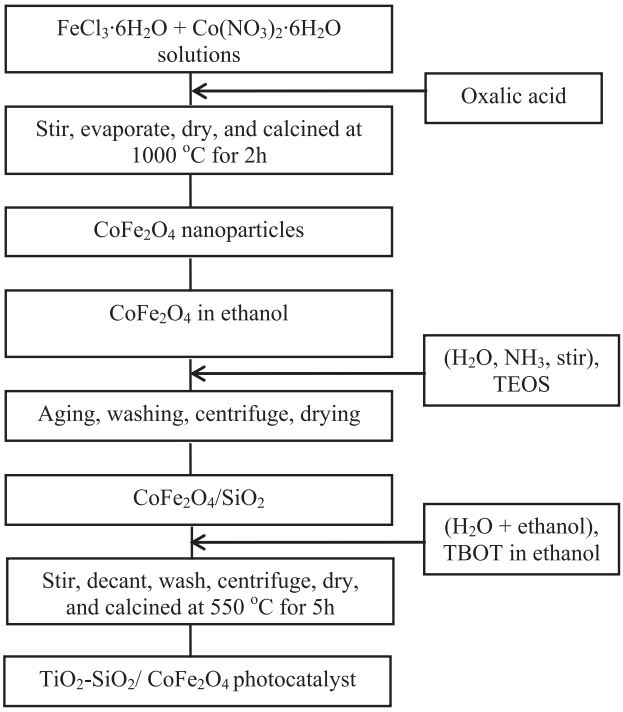

Fig. 1. Schematic flowchart for the preparation of TiO_2–SiO_2/$CoFe_2O_4$ magnetic photocatalyst.

then conducted via a two steps as follows. *First step*: coating of $CoFe_2O_4$ with silica via dispersing $CoFe_2O_4$ powder in absolute ethanol followed by adding the amount of H_2O required for the hydrolysis process and stirring for 10 min. Ammonia solution was then added to the mixture under vigorous stirring for another 10 min. A stiochoimetric ratio from tetraethyl orthosilicate TEOS ($Si(OC_2H_5)_4$) was dropped into the above solution. The solution was consequently aged for 5 h for a complete precipitation of silica. The product was washed using water and ethanol, then centrifuged and dried at 60 °C for 24 h in an oven. *Second step*: coating the Co-ferrite/SiO_2 with TiO_2. The product of first step (0.125 g) was dispersed in 25 ml ethanol in an ultrasonic bath for 30 min. at a temperature 20 °C, transferred the dispersion to a mixture of ethanol and water, 35 ml+25 ml, respectively. An amount of TBOT (titanium (IV) butoxide, $C_{16}H_{36}O_4Ti$) in 40 ml of ethanol is then transferred dropwise to the above mixture. The solution was kept under vigorous stirring for 3 h at room temperature, followed by a decantation overnight. The final product was then washed by water and ethanol, centrifuged and dried for 2 days at 60 °C in an oven, followed by calcination at 550 °C for 5 h. The choice of calcination temperature and time is selected accordingly to our previous report [32].

2.2. Catalyst characterization

The as-produced catalysts were evaluated and characterized using different techniques. The phase and crystal structure of the catalysts were obtained using X-ray powder diffraction (XRD) using a model Bruker axis diffractometer (D8-ADVANCE) with Cu Kα radiation, operating at 40 kV and 30 mA with a rate of 2°/min. X-ray photoelectron spectroscopy

(XPS) studies were performed using a Thermo Scientific K-ALPHA, XPS, England. The recorded binding energies have been calibrated by taking the C1s peak at 285.0 eV as a reference. The morphology of $CoFe_2O_4$ and as-synthesized catalyst was observed by scanning electron microscopy (JEOL-JSM 6400 SEM) and transmission electron microscope (JEOL-JSM 5400 TEM), coupled with energy dispersive X-ray spectroscopy (EDX) for further chemical analysis. Fourier transform infrared spectroscopy (FT-IR) was conducted on a Thermo Electron Magna 760. Pellets were made using potassium bromide (KBr), 99% purity FT-IR grade (Sigma-Aldrich). Powders were added to KBr in a mass ratio of 1:100. The magnetic properties of the produced ferrite powders were characterized using a vibrating sample magnetometer (VSM; 9600-1 LDJ, USA) at room temperature in a maximum applied field of 15 kOe. From the obtained hysteresis loops, the saturation magnetization (*Ms*), remanence magnetization (*Mr*) and coercivity (*Hc*) were consequently determined. The specific surface area S_{BET} of the samples was measured by nitrogen adsorption–desorption technique (Quantachrome instrument model Nova 2000 series). N_2-adsorption measurement was carried out at 77 K. Outgasing was done at 250 °C overnight prior to analysis.

2.3. Photocatalytic activity

The photodegradation experiments were performed in an aqueous solution containing methylene blue (MB) dye $C_{16}H_{18}N_3SCl$. A quartz photoreactor was filled with 300 ml aqueous solution of MB at various concentrations ranging from 100 to 250 ppm. The catalyst loading was varied from 0.033 to 0.333 g/l in 300 ml dye solutions. UV irradiation was applied using a 150 W medium pressure xenon lamp immersed in a quartz jacket and equipped with a cooling tube. The catalytic reaction was conducted at room temperature. Prior to the illumination, the adsorption equilibrium of dye in the presence of desired catalyst loading was attained in the dark during 30 min. In the continuous recirculation mode experiments, aliquots (5 ml) were retrieved from the reservoir at certain time intervals and analyzed after filtering through (0.2 mm) Millipore filter. The concentration of unreacted MB dye was analyzed using UV JASCO (V570) spectrophotometer at $\lambda_{max}=612$ nm. The photocatalytic activity was calculated by applying the following equation:

$$\% \text{ Photocatalytic activity} = [(C_o - C)/C_o] \times 100$$

where C_o is the initial dye concentration after equilibration in the dark and C is the dye concentration after photodegradation.

3. Results and discussion

3.1. Synthesis and characterization of TiO_2–SiO_2/$CoFe_2O_4$ photocatalyst

Cobalt ferrite, as a magnetic part, was initially prepared via oxalic acid precursor method. Fig. 2(a) and (b) show, respectively the SEM micrograph of as-synthesized $CoFe_2O_4$ with the corresponding magnetic hysteresis loop. As can be seen, the ferrite particles have regular cubic-like structure with agglomeration. Most of particles are homogeneous, uniform structure with narrow size distribution. The saturation magnetization obtained, Fig. 2(b), was found to be 67.74 emu/g, which is smaller than the corresponding bulk value (about 80 emu/g). The lower in saturation magnetization is likely associated with nanocrystalline $CoFe_2O_4$ powder that may lead to structural distortions in the surface compared to the bulk material.

The coating of as-synthesized $CoFe_2O_4$ using TiO_2–SiO_2 via a two-step sol–gel approach was conducted. The molar ratio of silica/cobalt ferrite was found to be a crucial factor determining the microstructure and morphology of as-synthesized magnetic nanocomposites, and thus a series of experiments was performed by changing the silica/cobalt ferrite molar ratios from 0.004 to 0.032. The experiments were conducted at constant ethanol/cobalt ferrite molar ratio 15, ammonia/cobalt ferrite molar ratio 0.8, TBOT/ethanol molar ratio 0.0025. Fig. 3 shows X-ray diffraction patterns of as-prepared $CoFe_2O_4$ as well as the patterns related to titania–silica/cobalt ferrite samples prepared at different silica/cobalt ferrite molar ratios (0.004, 0.008, 0.016 and 0.032).

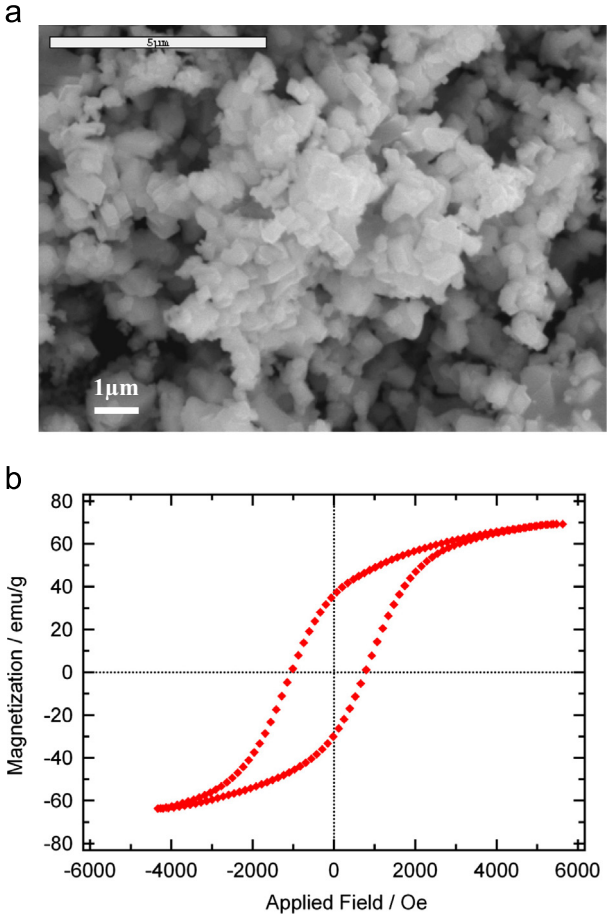

Fig. 2. SEM micrograph of cobalt ferrite synthesized by oxalic acid precursor method with Fe^{3+}/Co^{2+} molar ratio of 2:1 and annealed at 1000 °C for 2 h (a) and the corresponding *M–H* hysteresis loop (b).

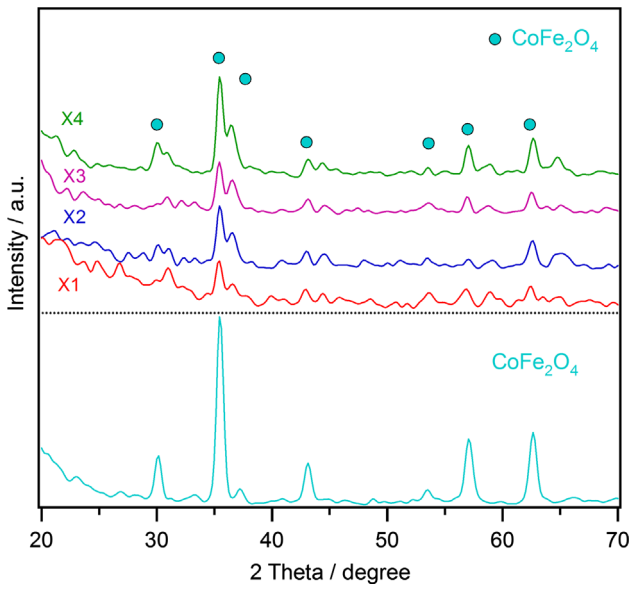

Fig. 3. X-ray diffraction patterns of as-synthesized $CoFe_2O_4$ (bottom pattern) and titania–silica/cobalt ferrite nanocomposites (top patterns) prepared at different silica/cobalt ferrite molar ratios: $X1=0.004$, $X2=0.008$, $X3=0.016$, and $X4=0.032$.

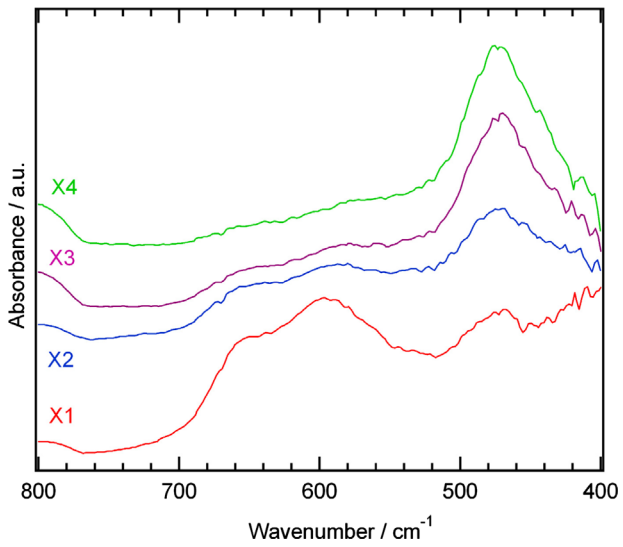

Fig. 4. FT-IR spectra of titania–silica/cobalt ferrite nanocomposites prepared at different silica/cobalt ferrite molar ratios: $X_1=0.004$, $X_2=0.008$, $X_3=0.016$, and $X_4=0.032$.

Bragg reflections for the $CoFe_2O_4$ (Fig. 3, bottom pattern) particles can be indexed to a pure spinel phase (JCPDS card # 79-1744) with a good crystalline state. The mean crystallite size (D) of $CoFe_2O_4$ particles is close to 87.9 nm based on the Debye–Scherrer formula ($D=0.89\lambda/\beta\cos\theta$), where λ is the X-ray wavelength, θ the Bragg angle, and β the full-width at half-maximum) [33]. The XRD patterns for magnetic nanocomposites (Fig. 3, top patterns), at different molar ratios, show evidently reduced line intensities of $CoFe_2O_4$. It is very hard to detect the bands ascribing to the characteristic anatase TiO_2 phase. The absence of anatase TiO_2 likely indicates a crystallization delay of TiO_2 phase which is probably due to the high concentration of SiO_2 in the catalyst. Such low crystallinity of TiO_2 under similar calcination conditions is consistent with a previously reported data for ZnO/TiO_2–SiO_2 system [34]. It is worthy to note that the crystallinity of magnetic $CoFe_2O_4$ nanoparticles is retained, to some extent, after the coating with TiO_2–SiO_2, and this is the case often observed for SiO_2-coated spinel ferrite [35].

The presence of TiO_2 in catalyst is further confirmed by XPS. Fig. 4 gives the wide-scan as well as the narrow (high resolution) scan XPS spectra of the catalyst. As demonstrated in the top spectra of Fig. 4, the catalyst contains Si, Ti, O, Fe and Co elements, in addition to C. The carbon on catalyst surface originates from contamination due to handling or pumping oil. The high resolution narrow-scan XPS spectra of Ti2p, Si2p, Co2p, Fe2p and O1s peaks for TiO_2–SiO_2/$CoFe_2O_4$ sample are shown in Fig. 4 (bottom). The Ti2p *XP* spectra indicate the presence of spin orbit components $2p_{3/2}$ and $2p_{1/2}$ for the TiO_2 observed at 459.11 and 464.56 eV, respectively, corresponding to Ti^{4+} (the highest oxidation state of Ti) [36]. The core-level spectra of Si2p and O1s in catalyst are detected at binding energies of 103.57 and 532.87 eV, respectively, which are consistent with previous studies [37–39]. There is no shift in binding energy for Si2p, which indicates no significant change in the chemical environment of the TiO_2/SiO_2 composite oxide. The Fe2p core-electron spectrum in $CoFe_2O_4$ is detected at 714.9 eV, which can be ascribed to Fe^{3+} ions in tetrahedral sites [40]. In addition, characteristic Co2p core-level spectra are observed, with binding energies of $Co2p_{3/2}$ at 781.3 eV and $Co2p_{1/2}$ at 796.9 eV. The binding energy difference between $Co2p_{3/2}$ and $Co2p_{1/2}$ is 15.6 eV which compares well with the value of 15.7 eV reported earlier for Co^{2+} in $CoAl_2O_4$ [41]. It can be also seen that the main peaks ($Co2p_{3/2}$ and $Co2p_{1/2}$) exhibit an obvious shoulder at their-energy side. Such strong shoulder is related to the shake-up process of Co^{2+} in the high-spin state [42].

FT-IR spectra of titania–silica/cobalt ferrite nanocomposites prepared at different silica/cobalt ferrite molar ratios are shown in Fig. 5. The ferrite related bands usually appear where the high wave number band υ_1 at 500–650 cm^{-1} is assigned to the tetrahedral complexes, whereas the lower υ_2 at 400–470 cm^{-1} is assigned to the octahedral complexes. Therefore in the investigated samples, the absorption broad bands observed around 467 and 603 cm^{-1} could be assigned to the stretching vibrations of the M–O (M=Fe, Co) bands in $CoFe_2O_4$ compounds. The high frequency band around 603 cm^{-1} could be attributed to the tetrahedral complex (Fe^{3+}–O^{2-}) and the variation in the band position of υ_1 and υ_2 is due to the difference in the Fe^{3+}–O^{2-} distances for the tetrahedral and octahedral sites [31].

The magnetic properties together with the specific surface area and degradation removal efficiency of MB using the magnetic nanocomposites prepared at different silica/cobalt ferrite molar ratios are shown in Table 1. The obtained results revealed that all coated samples could be regarded as moderate hard ferromagnetic materials due to their high coercive force ranging from 299 to 484 Oe and remanence values ranging from 3.9 to 14.1 emu/g. The saturation magnetizations

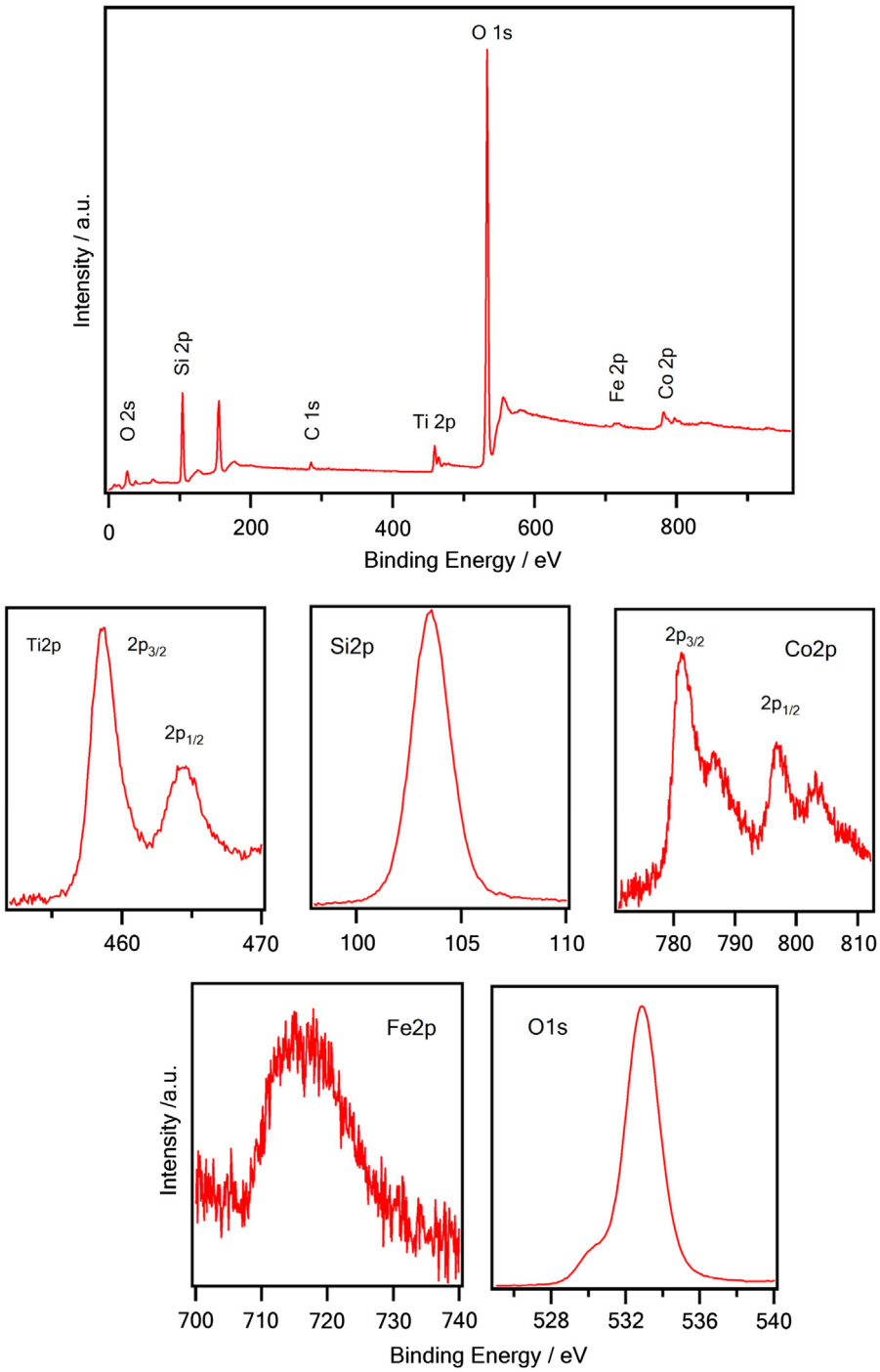

Fig. 5. Wide-scan (top) and narrow-high resolution scan XPS spectra of the TiO_2–SiO_2/$CoFe_2O_4$ catalyst. The high resolution scan spectra were measured for the Ti2p, Si2p, Co2p, Fe2p and O1s.

obtained for nanocomposites are smaller than the value obtained for pure $CoFe_2O_4$ sample, Fig. 2(b). The reduction of magnetization of TiO_2–SiO_2 coated $CoFe_2O_4$ compared to the uncoated $CoFe_2O_4$ nanoparticles is related to the contribution of the volume of the non-magnetic coating layer to the total volume of sample. The non-magnetic SiO_2–TiO_2 coating layer can act as a magnetically dead layer on $CoFe_2O_4$ surface, and hence affecting the magnetization due to quenching of surface moments [22]. The highest saturation magnetization $Ms = 43.5$ emu/g, remanence magnetization (Mr) and coercivity (Hc) are detected at silica/cobalt ferrite molar ratio 0.016 (sample $X3$). This implies that the separation of catalyst from the suspension can be easily magnetized and consequently the photocatalyst can be re-dispersed in a solution for re-using.

The presented data of Table 1 also revealed that an increase in the silica/cobalt ferrite molar ratio from 0.004 to 0.016 led to an increase in the surface area from 300 to 460 m^2/g and the MB degradation efficiency from 78.7% to 98.3%. This means,

Table 1
Magnetic properties, specific surface area, and dye degradation efficiency for the magnetic nanocomposites prepared at different silica/cobalt ferrite molar ratios.

Sample number	Silica/cobalt ferrite molar ratio	*Ms*, emu/g	*Mr*, emu/g	*Hc*, Oe	Specific surface area, S_{BET}, m^2/gm	Degradation efficiency, %
*X*1	0.004	38.3	11.3	299	300	78.7
*X*2	0.008	22.9	5.1	332	380	93.7
*X*3	0.016	43.5	14.1	484	460	98.3
*X*4	0.032	15.8	3.9	299	466	98

the increased silica content caused an increase in the surface area. However, there is no significant effect on the surface area and the degradation efficiency with further increase in silica/cobalt ferrite molar ratio above 0.016. This result reveals that appropriate content of silica and $CoFe_2O_4$ should be adjusted for achieving appropriate surface area for the final catalyst. As the concentration of magnetic part as seed particles is monitored, this could provide appropriate surface nucleation sites for silica that essentially occurred at high silica/cobalt ferrite molar ratio.

The morphology of magnetic nanocomposites prepared at different silica/cobalt ferrite molar ratios was further observed with TEM. The recorded images are shown in Fig. 6, along with the corresponding EDX chemical analysis depicted in graph (e). The TEM micrograph of Fig. 6(a) clearly shows that the $CoFe_2O_4$ nanoparticles are dispersed in SiO_2 coating matrix. Increasing silica/cobalt ferrite molar ratio from 0.004 to 0.008 enhanced the precipitation of SiO_2 in a shell like structure, while the $CoFe_2O_4$ nanoparticles started to agglomerate and encapsulate inside SiO_2 matrix (Fig. 6(b). Further increase in silica/cobalt ferrite molar ratio to 0.016 led to the formation of a core–shell like structure, where the precipitated silica with some adhered TiO_2 nanoparticles coating represent the shell and $CoFe_2O_4$ is the core, Fig. 6(c). Increasing the silica/cobalt ferrite molar to 0.032 led to the separation of titania–silica shell from the magnetic core, Fig. 6(d), probably due to the increased attraction force between silica and titania. The EDX analysis shown in Fig. 6(e) reveals that the as-formed catalyst consists mainly of Co, Fe, Ti, Si and O elements, which are the main constituents of the TiO_2–SiO_2/$CoFe_2O_4$ sample. The spectra detected for Cu element come from the Cu grid used for the analysis.

It seems that the formation of a core–shell like structure is essentially dependent on the molar ratio of core and shell forming materials and the interaction between them. The optimal silica/cobalt ferrite molar ratio is taken as 0.016, producing a core–shell structure and leading to a maximum degradation of MB. At optimal silica/cobalt ferrite molar ratio, the enhanced photodegradation efficiency of MB could be ascribed to the high surface area of catalyst as well as the core–shell structure. $CoFe_2O_4$ core would likely act as an effective recombination center for the photogenerated electrons and holes. It has been reported previously that the photocatalytic performance could be improved by depositing silica layer between titania and magnetic iron oxide [21,43]. For the current photocatalyst, SiO_2 layer between $CoFe_2O_4$ and TiO_2 may prevent the charge injection from semiconductor TiO_2 to magnetic $CoFe_2O_4$, which in turn lead to the increase in photocatalytic activity.

3.2. Factors influencing MB degradation

3.2.1. Effect of pH

Generally, the solution pH is an important operational variable in wastewater treatment and is a key factor influencing the photocatalytic degradation process of organic compounds. The influence of pH on the degradation of MB was studied at pH values 2–9. The initial dye concentration was 100 ppm, using 50 mg catalyst in 300 ml solution (0.165 g/L) for 40 min. The effect on MB photodegradation is shown in Table 2. The degradation efficiency of MB increased gradually with increasing the pH value from acidic to alkaline direction. Similar behavior has been reported previously using TiO_2–SiO_2 photocatalyst [44]. The pH essentially influences the surface charge properties of photocatalyst. In alkaline solution, TiO_2 surface is presumably negatively charged, while it is positively charged in acidic solution. MB is a cationic dye and thus it has a high tendency to be adsorbed onto the TiO_2 surface at alkaline pH. This is the reason why the highest degradation of 98.3% was achieved at pH 9, while a degradation efficiency of only 49.2% was obtained at acidic pH 2. This result indicates that the photodegradation process likely occurs at the catalyst surface and not in bulk solution. In addition, one would expect that the interaction between the photogenerated holes and hydroxide ions (OH^-) to generate hydroxyl radicals ($OH^\bullet$) is enhanced in alkaline pH, which in turn would facilitate the photocatalytic degradation of MB.

3.2.2. Effect of initial concentration of MB

The effect of initial concentration of MB on the degradation efficiency was examined using various dye concentrations from 100 to 250 ppm with a constant catalyst loading 0.165 g/L at pH 9 for 40 min irradiation time. As a general trend in Table 2 the photodegradation efficiency decreased with increasing dye concentration. The crucial factor controlling the photodegradation of MB is the formation of hydroxyl radicals on catalyst surface as well as the interaction of such radicals with dye species. As the initial concentration of dye increased, much more dye molecules are adsorbed on catalyst surface, and hence the generation of hydroxyl radicals would be reduced since the majority of active sites is covered by dye molecules. As a result, the photodegradation efficiency decreased. Furthermore, it is likely that at a high concentration of dye, a shielding effect for light passing into solution is attained, which in turn reduced the

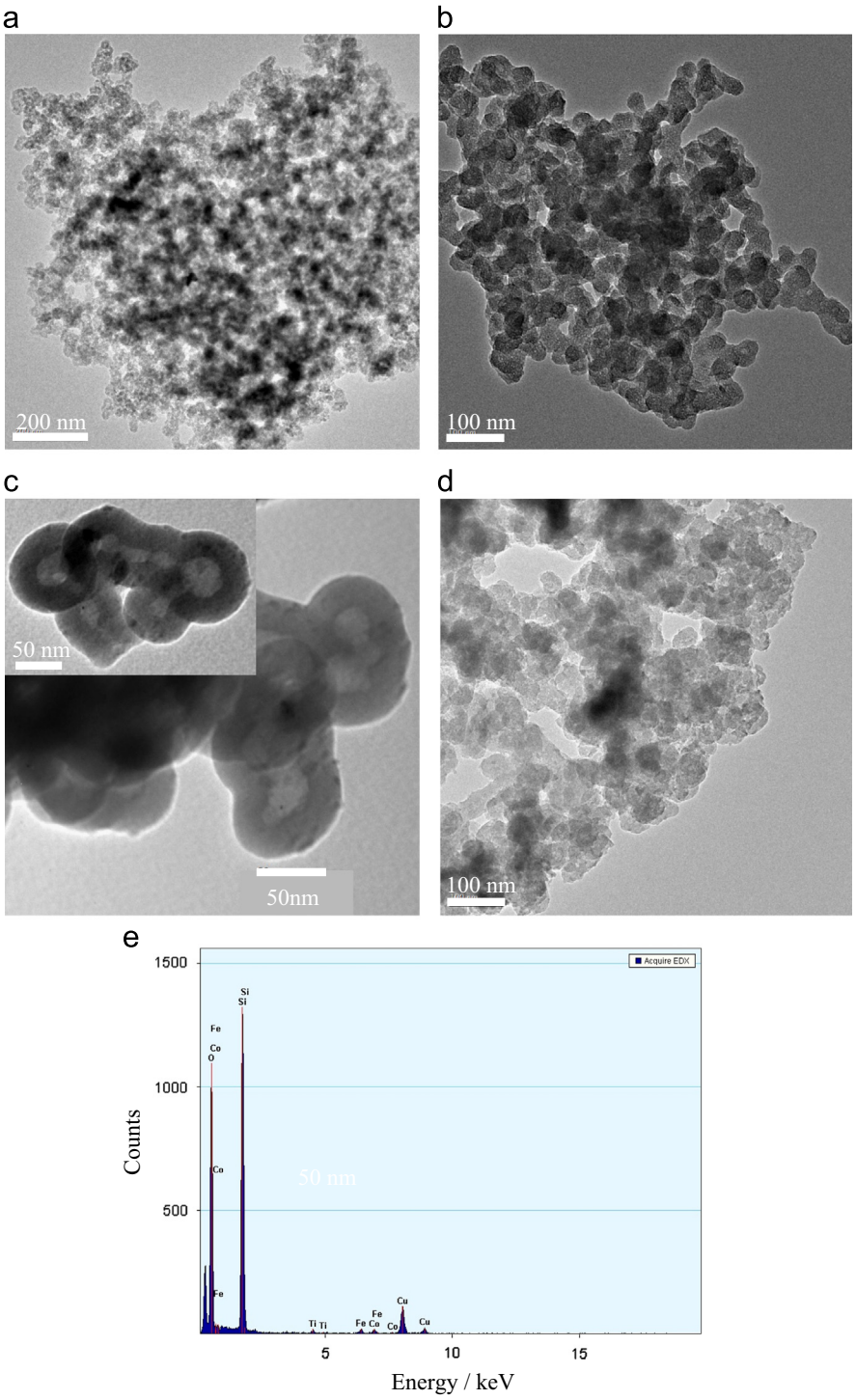

Fig. 6. TEM images of titania–silica/cobalt ferrite nanocomposites prepared at different silica/cobalt ferrite molar ratios; (a) 0.004, (b) 0.008, (c) 0.016 and (d) 0.032. The corresponding EDX analysis of sample (c) is shown in graph (e).

absorption of photons by catalyst, and thus the hydroxyl radicals formed on catalyst surface would decrease.

3.2.3. *Effect of catalyst loading*

The effect of catalyst loading on MB degradation was further investigated using 0.033, 0.083, 0.165, 0.248, 0.333 g/L catalyst in 100 ppm MB solution at pH 9 and a sample of the reaction mixture was taken for analysis at different irradiation times (3–60 min). The results are shown in Fig. 7. Control experiments were also conducted under UV illumination and in absence of catalyst to gain better understanding whether photolysis takes place for MB dye. As shown in Fig. 7, photolysis of dye was 21% after 40 min. illumination time without the photocatalyst. At all catalyst loadings, the photodegradation efficiencies were found to increase gradually with increasing reaction

Table 2
Effect of solution pH and initial concentration of MB on photocatalytic degradation of MB dye.

pH value/MB concentration, ppm	Degradation efficiency, %
2/100	49.2
4/100	59
7/100	88.5
9/100	98.3
9/150	93.5
9/200	88.5
9/250	70.0

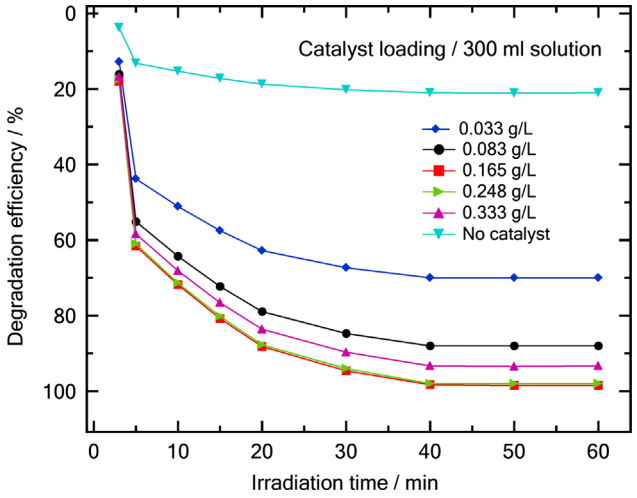

Fig. 7. Effect of different catalyst loadings on MB degradation. Conditions: MB initial concentration: 100 ppm; 300 ml dye solution; pH 9 at room temperature; 30 min. adsorption.

time, reaching the maximum degradation efficiency at 40 min. As the catalyst loading increased from 0.033 to 0.083 g/L, an increase in degradation efficiency from 70% to 88% was observed. Further increase in catalyst loading to 0.165 g/L led to an increase in degradation to its optimal value of 98.3% after 40 min illumination. No further increase in degradation was detected using 0.248 g/L catalyst. Meanwhile, at 0.333 g/L loading, the photocatalytic degradation decreased again to 93.3% (5% drop in efficiency) after 40 min reaction time and under the same experimental conditions. Thus, the catalyst loading for maximum degradation of MB is 0.165 g/L in 300 ml dye solution. The increase in catalyst loading is accompanied by an increase in the number of active sites on the photocatalyst surface, which in turn increased the formation rate of hydroxyl radicals. When the catalyst loading exceeded the limiting value, the MB degradation rate would decrease, due to the interception of light by the suspension. Aggregation of catalyst particles is expected at high catalyst loading, causing a reduction in surface active sites, increasing light scattering and finally leading to decrease in the passage of irradiation through the samples [45].

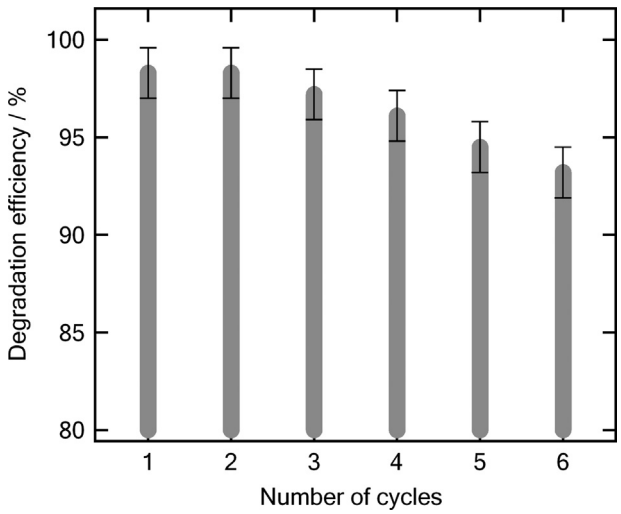

Fig. 8. Recycling of catalyst. Catalyst loading 0.165 g/L, initial MB concentration 100 ppm, 300 ml dye solution, pH 9 at room temperature.

3.3. Recycling of photocatalyst

Recycling of catalysts is one of the key steps to assess the practical application of photocatalysts and to develop heterogeneous photocatalysis technology for wastewater treatment. An examination of the photocatalytic activity of the recycled $CoFe_2O_4/SiO_2$–TiO_2 catalyst by a magnetic field was carried out. The separated photocatalyst was utilized to photodegrade the MB repeatedly under UV irradiation. The photocatalytic degradation efficiency was 98.3% during the first 2 cycles (Fig. 8). The catalyst activity slightly dropped in runs 3 and 4, giving 97.2% and 96.1% degradation, respectively. In the 5th run, the catalyst showed 94.5% degradation. At run 6, a degradation efficiency of 93.2% was obtained. The deactivation of the photocatalyst is likely related to some surface poisoning that may be induced by adsorbed intermediates. The experimental observation of Dutta and Ray [46] indicated that strongly adsorbed intermediates occupied the active sites on the catalyst surface and led to the loss of photocatalytic activity. The results reveal that the separation of photocatalyst by the magnetic field is effective and thus the magnetic photocatalyst is basically stable and is promising for environmental remediation.

4. Conclusions

Magnetic nanocomposites of titania coating on silica-modified cobalt ferrite have been successfully synthesized. The magnetic cobalt ferrite was synthesized using the organic acid precursor method, followed by coating the magnetic surface by SiO_2 and TiO_2 via a two-step sol gel technique. It was found that controlling the coating process of cobalt ferrite by titania–silica are crucial steps for obtaining appropriate catalytic performance of the catalyst. The as-synthesized nanocomposites were examined for the degradation of methylene blue dye in an aqueous solution. Based on the results achieved, it is concluded that the photocatalytic degradation of dye is dependent on the catalyst loading, solution pH and the

initial dye concentration. Best performance for dye degradation with efficiency reached 98.3% was achieved using 0.165 g/L catalyst in 300 ml solution with dye concentration 100 ppm at alkaline pH 9 during 40 min. The magnetic properties of the catalyst permit the efficient separation of dispersed catalyst from the treated solutions. The results of catalyst re-use revealed the present magnetic photocatalyst remain effective and active after six cycles, which indicate the promising recyclability of TiO_2–SiO_2/$CoFe_2O_4$ photocatalyst. The present magnetic photocatalyst is expected to demonstrate a broad range of utility for other catalytic reactions which needs further investigation.

Acknowledgements

We acknowledge the help of Major Analytical Instrumentation Center (MAIC) at the Materials Science and Engineering Department of the University of Florida for TEM and FT-IR measurement. This work was supported by the Egyptian Science and Technology Developing Fund (STDF) and the US National Science Foundation through US-Egypt Joint Science and Technology Fund under the Grant no. ID 427.

References

[1] Y. Ao, J. Xu, D. Fu, X. Shen, C. Yuan, A novel magnetically separable composite photocatalyst: titania-coated magnetic activated carbon, Separation and Purification Technology 61 (2008) 436–441.

[2] T. Ung, L.M. Liz-Marzan, P. Mulvaney, Optical properties of thin films of Au@SiO_2 particles, Journal of Physical Chemistry B 105 (2001) 3441–3452.

[3] C. Wang, Y. Ao, P. Wang, J. Hou, J. Qian, A facile method for the preparation of titania-coated magnetic porous silica and its photocatalytic activity under UV or visible light, Colloids and Surfaces A: Physicochemical and Engineering Aspects 360 (2010) 184–189.

[4] J.Y. Lee, J.H. Lee, S.H. Hong, Y.K. Lee, J.Y. Choi, Coating $BaTiO_3$ nanolayers on spherical Ni powders for multilayer ceramic capacitors, Advanced Materials 15 (2003) 1655–1658.

[5] V. Jokanovic´, A.M. Spasic´, D. Uskokovic´, Designing of nanostructured hollow TiO_2 spheres obtained by ultrasonic spray pyrolysis, Journal of Colloid and Interface Science 278 (2004) 342–352.

[6] J. Yin, X. Qian, J. Yin, M. Shi, J. Zhang, G. Zhou, Preparation of polystyrene/zirconia core-shell microspheres and zirconia hollow shells, Inorganic Chemistry Communications 6 (2003) 942–945.

[7] D.A. Tryk, A. Fujishima, K. Honda, Recent topics in photoelectrochemistry: achievements and future prospects, Electrochimica Acta 45 (2000) 2363–2376.

[8] M. Alvaro, B. Cojocaru, A.A. Ismail, N. Petrea, B. Ferrer, F.A. Harraz, V.I. Parvulescu, H. Garcia, Visible-light photocatalytic activity of gold nanoparticles supported on template-synthesized mesoporous titania for the decontamination of the chemical warfare agent SOMAN, Applied Catalysis B: Environmenta 99 (2010) 191–197.

[9] M. Pera-Titus, V. Garcona-Molina, M. Banos, J. Gimenez, S. Esplugas, Degradation of chlorophenols by means of advanced oxidation processes: a general review, Applied Catalysis B: Environmental 47 (2004) 219–256.

[10] A. Mills, S. Hunte, An overview of semiconductor photocatalysis, Journal of Photochemistry and Photobiology A 108 (1997) 1–35.

[11] J. Herrmann, Heterogeneous photocatalysis: fundamentals and applications to the removal of various types of aqueous pollutants, Catalysis Today 53 (1999) 115–129.

[12] R.M. Mohamed, F.A. Harraz, I.A. Mkhalid, Hydrothermal synthesis of size-controllable yttrium orthovanadate (YVO_4) nanoparticles and its application in photocatalytic degradation of direct blue dye, Journal of Alloys and Compounds 532 (2012) 55–60.

[13] K. Lv, Q. Xiang, J. Yu, Effect of calcination temperature on morphology and photocatalytic activity of anatase TiO_2 nanosheets with exposed {001} facets, Applied Catalysis B: Environmental 104 (2011) 275–281.

[14] G.M. Liu, X.Z. Li, J.C. Zhao, H. Hidaka, N. Serpone, Photooxidation pathway of sulforhodamine-B: dependence on the adsorption mode on TiO_2 exposed to visible light radiation, Environmental Science and Technology 34 (2000) 3982–3990.

[15] M. Anpo, Utilization of TiO_2 photocatalysts in green chemistry, Pure and applied chemistry Chimie pure et appliquée 72 (2000) 1265–1270.

[16] J.C Crittenden, J.B. Liu, D.W. Hand, D.L. Perram, Photocatalytic oxidation of chlorinated hydrocarbons in water, Water Research 31 (1997) 429–438.

[17] K. Sopajaree, S.A. Qasim, S. Basak, K. Rajeshwar, An integrated flow reactor-membrane filtration system for heterogeneous photocatalysis. Part II: experiments on the ultrafiltration unit and combined operation, Journal of Applied Electrochemistry 29 (1999) 1111–1118.

[18] F.A. Harraz, O.A. Abdel-Salam, A.A. Mostafa, R.M. Mohamed, M. Hanafy, Rapid synthesis of titania–silica nanoparticles photocatalyst by a modified sol–gel method for cyanide degradation and heavy metals removal, Journal of Alloys and Compounds 551 (2013) 1–7.

[19] D. Beydoun, R. Amal, Implications of heat treatment on the properties of a magnetic iron oxide–titanium dioxide photocatalyst, Materials Science and Engineering B 94 (2002) 71–81.

[20] S. Rana, R.S. Srivastava, M.M. Sorensson, R.D.K. Misra, Synthesis and characterization of nanoparticles with magnetic core and photocatalytic shell: anatase TiO_2–$NiFe_2O_4$ system, Materials Science and Engineering B 119 (2005) 144–151.

[21] F. Chen, Y.D. Xie, J.C. Zhao, G.X. Lu, Photocatalytic degradation of dyes on a magnetically separated photocatalyst under visible and UV irradiation, Chemosphere 44 (2001) 1159–1168.

[22] M. Ma, Y. Zhang, X. Li, D. Fu, H. Zhang, N. Gu, Synthesis and characterization of titania-coated Mn–Zn ferrite nanoparticles, Colloids and Surfaces A: Physicochemical and Engineering Aspects 224 (2003) 207–212.

[23] D. Beydoun, R. Amal, G. Low, S. McEvoy, Occurrence and prevention of photodissolution at the phase junction of magnetite and titanium dioxide, Journal of Molecular Catalysis A: Chemical 180 (2002) 193–200.

[24] Y. Ao, J. Xu, D. Fu, C. Yuan, Photocatalytic degradation of X-3B by titania-coated magnetic activated carbon under UV and visible irradiation, Journal of Alloys and Compounds 471 (2009) 33–38.

[25] W.S. Lee, J. Drwiega, D. Mazyck, Y.C. Wu, M.W. Sigmund, Synthesis and characterization of hard magnetic composite photocatalyst-Barium ferrite/silica/titania,, Materials Chemistry and Physics 96 (2006) 483–488.

[26] F.A. Harraz, Polyethylene glycol-assisted hydrothermal growth of magnetite nanowires: synthesis and magnetic properties, Physica E: Low-Dimensional Systems and Nanostructures 40 (2008) 3131–3136.

[27] S.M. El-Sheikh, F.A. Harraz, M.M. Hessien, Magnetic behavior of cobalt ferrite nanowires prepared by template–assisted technique, Materials Chemistry and Physics 123 (2010) 254–259.

[28] S.M. El-Sheikh, F.A. Harraz, K.A. Saad, Catalytic performance of nanostructured iron oxides synthesized by thermal decomposition technique, Journal of Alloys and Compounds 487 (2009) 716–723.

[29] Y.S. Chung, S.B. Park, D.W. Kang, Magnetically separable titania-coated nickel ferrite photocatalyst, Materials Chemistry and Physics 86 (2004) 375–381.

[30] H. Zhang, R. Hou, Z.-L. Lu, X. Duan, A novel magnetic nanocomposite involving anatase titania coating on silica-modified cobalt ferrite via lower temperature hydrolysis of a water-soluble titania precursor, Materials Research Bulletin 44 (2009) 2000–2008.

[31] R.M. Mohamed, M.M. Rashad, F.A. Harraz, W. Sigmund, Structure and magnetic properties of nano-crystalline cobalt ferrite powders synthesized using organic acid precursor method, Journal of Magnetism and Magnetic Materials 322 (2010) 2058–2064.

[32] A.A. Ismail, I.A. Ibrahim, M.S. Ahmed, R.M. Mohamed, H. El-Shall, Sol–gel synthesis of titania–silica photocatalyst for cyanide photodegradation, Journal of Photochemistry and Photobiology A: Chemistry 163 (2004) 445–451.
[33] C. Hammond, The Basics of Crystallography and Diffraction, Oxford University Press, Oxford, 1997.
[34] A.A. Ismail, Single-step synthesis of a highly active photocatalyst for oxidation of trichloroethylene, Applied Catalysis B: Environmental 85 (2008) 33–39.
[35] D.K. Yi, S.T. Selvan, S.S. Lee, G.C. Papaefthymiou, D. Kundaliya, J.Y. Ying, Silica-coated nanocomposites of magnetic nanoparticles and quantum dots, Journal of the American Chemical Society 127 (14) (2005) 4990–4991.
[36] J.T. Mayer, U. Diebold, T.E. Madey, E. Garfunkel, Titanium and reduced titania overlayers on titanium dioxide (110), Journal of Electron Spectroscopy 73 (1995) 1–11.
[37] Y.H. Ogata, J. Sasano, J. Jorne, T. Tsuboi, F.A. Harraz, T. Sakka, Immersion plating of copper on porous silicon in various solutions, Physica Status Solidi (A) 182 (2000) 71–77.
[38] F.A. Harraz, J. Sasano, T. Sakka, Y.H. Ogata, Different behavior in immersion plating of nickel onto porous silicon from acidic and alkaline fluoride media, Journal of the Electrochemical Society 150 (2003) C277–C284.
[39] F.A. Harraz, T. Sakka, Y.H. Ogata, Immersion plating of copper using $(CF_3SO_3)_2Cu$ onto porous silicon from organic solutions, Electrochimica Acta 46 (2001) 2805–2810.
[40] Z. Zhou, Y. Zhang, Z. Wang, W. Wei, W. Tang, J. Shi, R. Xiong, Electronic structure studies of the spinel $CoFe_2O_4$ by X-ray photoelectron spectroscopy, Applied Surface Science 254 (2008) 6972–6975.
[41] J.G. Dillard, C.V. Schenck, M.H. Koppelman, Surface chemistry of cobalt in calcined cobalt–kaolinite materials, Clays and Clay Minerals 31 (1983) 69–72.
[42] W. Huang, Z. Zuo, P. Han, Z. Li, T. Zhao, XPS and XRD investigation of $Co/Pd/TiO_2$ catalysts by different preparation methods, Journal of Electron Spectroscopy 173 (2009) 88–95.
[43] D. Beydoun, R. Amal, G. Low, S. McEvoy, Novel photocatalyst: titania-coated magnetite. Activity and photodissolution, Journal of Physical Chemistry B 104 (2000) 4387–4396.
[44] C. Guillard, H. Lachheb, A. Houas, M. Ksibi, E. Elaloui, J.M Herrmann, Influence of chemical structure of dyes, of pH and of inorganic salts on their photocatalytic degradation by TiO_2 comparison of the efficiency of powder and supported TiO_2, Journal of Photochemistry and Photobiology A: Chemistry 158 (2003) 27–36.
[45] A.P. Toor, A. Verma, C.K. Jotshi, P.K. Bajpai, V. Singh, Photocatalytic degradation of direct yellow 12 dye using UV/TiO_2 in a shallow pond slurry reactor, Dyes and Pigments 68 (2006) 53–60.
[46] K.P. Dutta, A.K. Ray, Experimental investigation of taylor vortex photocatalytic reactor for water purification, Chemical Engineering Science 59 (2004) 5249–5259.